

CrystEngComm

Accepted Manuscript



This is an *Accepted Manuscript*, which has been through the Royal Society of Chemistry peer review process and has been accepted for publication.

Accepted Manuscripts are published online shortly after acceptance, before technical editing, formatting and proof reading. Using this free service, authors can make their results available to the community, in citable form, before we publish the edited article. We will replace this *Accepted Manuscript* with the edited and formatted *Advance Article* as soon as it is available.

You can find more information about *Accepted Manuscripts* in the [Information for Authors](#).

Please note that technical editing may introduce minor changes to the text and/or graphics, which may alter content. The journal's standard [Terms & Conditions](#) and the [Ethical guidelines](#) still apply. In no event shall the Royal Society of Chemistry be held responsible for any errors or omissions in this *Accepted Manuscript* or any consequences arising from the use of any information it contains.

Cite this: DOI: 10.1039/c0xx00000x

www.rsc.org/xxxxxx

ARTICLE

Metal(II) complexes based on 4-(2,6-di(pyridin-4-yl)pyridin-4-yl)benzonitrile: structures and electrocatalytic properties for hydrogen evolution reaction from water

Xiao Lin Gao,^a Yun Gong,^{*a} Pan Zhang,^a Yong Xi Yang,^a Jiang Ping Meng,^a Miao Miao Zhang,^a Jun Li Yin^a and JianHua Lin^{*a,b}

Received (in XXX, XXX) Xth XXXXXXXXX 20XX, Accepted Xth XXXXXXXXX 20XX

DOI: 10.1039/b000000x

Using a novel rigid ditopic ligand, 4-(2,6-di(pyridin-4-yl)pyridin-4-yl)benzonitrile (**L**), three metal(II)-complexes formulated as $M_2L_2(SO_4)_2(H_2O)_6 \cdot H_2O$ ($M=Ni$ (**1**), Co (**2**) and Cd (**3**)) have been solvothermally synthesized and structurally characterized by single-crystal X-ray diffraction. The three complexes are isostructural except for different metal(II) ions in the structures. They all show a one-dimensional (1D) chain, in which the **L** ligand acts a μ_2 -bridge linking two metal(II) centers. Different chains are connected by strong H bonds and π - π stacking interactions into three-dimensional (3D) supramolecular architecture. Among the three complexes, the Ni complex **1** and Co complex **2** can act as the electrocatalysts for hydrogen evolution reaction (HER) from water, and the Co complex **2** shows better electrocatalytic activity. In the present work, the graphene can't catalyze the HER, however, the complex **1**/graphene composite shows similar electrocatalytic activity to complex **1**. The three complexes show different UV-vis absorption, photoluminescence properties and thermal stabilities.

Introduction

In recent years, there is great interest in metal complexes not only because of their intriguing variety of structures, but also due to their interesting properties in catalysis, and porous materials, et al.¹ However, the electrochemical behaviors of metal complexes have not been extensively investigated.² In this regard, our recent study has been mainly focused on the synthesis and characterization of novel metal complexes, which show rich structural features and electrocatalytic properties for the H_2 evolution reaction (HER).³

In order to investigate the relationship between the species of metal(II) ions and the electrocatalytic activity for the HER, we synthesized a novel rigid ditopic ligand, 4-(2,6-di(pyridin-4-yl)pyridin-4-yl)benzonitrile (**L**) (**Scheme S1**).⁴ It is expected the ligand is stable under the electrochemical condition. In the present work, based on **L**, by changing metal(II) ions, we got three metal(II) complexes: $M_2L_2(SO_4)_2(H_2O)_6 \cdot H_2O$ ($M=Ni$ (**1**), Co (**2**) and Cd (**3**)). The three complexes are isostructural except for different metal(II) ions in the structures. The cyclic voltammograms (CVs), Tafel plots, electrochemical impedance spectroscopies (EISs), controlled potential electrolysis (CPE) experiments as well as UV-vis absorption spectra, photoluminescence properties and thermal stabilities of the three complexes have been investigated.

In order to lower the amount of metal complex for electrocatalysis, in the synthesis of complex **1**, graphene was added and the graphene/complex **1** composite was obtained. The electrocatalytic property of the graphene/complex composite for the HER from water has also been investigated.

Experimental Section

General Considerations All chemicals purchased were of

reagent grade and used without further purification. Graphene was purchased from Nanjing XFNANO Materials Tech Co., Ltd. C, H, N elemental analyses were performed on an Elementar Vario MICRO E III analyzer. IR spectra were recorded as KBr pellets on PerkinElmer spectrometer. The powder X-ray diffraction (XRD) data were collected on a RIGAKU DMAX2500PC diffractometer using $Cu K\alpha$ radiation. Raman spectra were conducted on a Nicolet iS50 Raman spectrometer. The morphologies of the samples were characterized by SEM (Model JSM-7600F, JEOL). UV-Vis spectra were measured on a HITACHI U-4100 UV-vis spectro-photometer. Solid-state photoluminescence spectra of all the compounds were measured at room temperature with a Cary Eclipse fluorescence spectrometer. TGA was performed on a NETZSCH STA 449C thermogravimetric analyzer in flowing N_2 with a heating rate of $10^\circ C \cdot min^{-1}$.

Electrochemical Measurements The electrochemical measurements were done in a three-electrode test cell using a Shiruisi RST5200 electrochemical workstation at $25^\circ C$. A saturated calomel electrode (SCE) and a platinum foil were used as the reference and counter electrode, respectively. The working electrode was prepared as follows: Firstly, a glassy carbon electrode (GCE) was polished by abrasive paper and aluminum oxide, then ultrasonically washed by ethanol, acetone and distilled water. Then an acetone dispersion of 4 mg complex or **L** (1 mL) and 0.05 mL of nafion were deposited on the GCE and the solvent is dried by an IR lamp. The electroactive geometric area of the GCE is 0.2 cm^2 . The measurements were recorded in 50 mL of N_2 degassed Na_2SO_4 (0.5 M) aqueous solution. The amount of H_2 evolved was determined using gas chromatography (GC, 7890A, thermal conductivity detector (TCD), Ar carrier, Agilent). Electrochemical impedance spectroscopy (EIS) measurements were conducted on CHI660E electrochemical

workstation in the range of 0.01 Hz - 1 MHz, and the experimental conditions of EIS are as follows: The amplitude of the potential perturbation is 0.005V. The frequency intervals are 100 K-1 M Hz, 10 K-100 K Hz, 1 K-10 K Hz, 100-1 K Hz, 10-100 Hz, 1-10 Hz, 0.1-1 Hz, 0.01-0.1 Hz. The number of points per frequency decade is 12. The time to stabilize the electrode/solution interface is 2s.

Synthesis of L: L was prepared according to the literature method.⁴ Melting point: > 250°C. IR (cm⁻¹): 3446.31(s), 3234.68(m), 3059.96(m), 2359.69(s), 2342.01(s), 2229.45(m), 1595.45(s), 1550.17(m), 1545.75(m), 1484.75(w), 1440.01(w), 1395.08(s), 825.28(s), 791.86(s), 691.94(w), 668.60(w), 648.83(m), 624.36(m), 503.53(w).

Synthesis of Ni₂L₂(SO₄)₂(H₂O)₆·H₂O (1): A mixture of NiSO₄·7H₂O (0.042 g, 0.15 mmol), L (0.018 g, 0.5 mmol), ethanol (4 ml) and H₂O (4 ml) were placed in a Teflon-lined stainless steel vessel and heated at 120 °C for 3 days, followed by cooling to room temperature. The resulting green block crystals were filtered off (yield: ca. 68 % based on L). Elemental Anal. Found: C, 47.82; N, 10.10; H, 3.78 %. Calcd. for C₄₄H₄₂N₈O₁₅S₂Ni₂: C, 47.85; N, 10.15; H, 3.81%. IR (cm⁻¹): 3239(s), 2229(m), 1611(s), 1558(w), 1541(m), 1505(w), 1479(w), 1397(m), 1114(s), 1064(s), 972(w), 863(w), 834(m), 808(m), 733(w), 686(m), 643(s), 507(w).

Synthesis of Co₂L₂(SO₄)₂(H₂O)₆·H₂O (2): The reaction procedure was carried out in a similar manner to that of **1**, except that CoSO₄ (0.42 g, 0.15 mmol) was used instead of NiSO₄·7H₂O (0.042 g, 0.15 mmol). The resulting red block crystals were filtered off (yield: ca. 72% based on L). Elemental Anal. Found: C, 47.80; N, 10.12; H, 3.76 %. Calcd. for C₄₄H₄₂N₈O₁₅S₂Co₂: C, 47.85; N, 10.15; H, 3.81%. IR (cm⁻¹): 3281(s), 2360(m), 2342(w), 2230(w), 1610(s), 1540(m), 1506(w), 1464(w), 1398(m), 1364(w), 1221(w), 1189(m), 1111(s), 1019(m), 987(w), 834(m), 743(w), 684(m), 642(s), 627(s), 505(w).

Synthesis of Cd₂L₂(SO₄)₂(H₂O)₆·H₂O (3): The reaction procedure was carried out in a similar manner to that of **1**, except that CdSO₄ (0.31 g, 0.15 mmol) was used instead of NiSO₄·7H₂O (0.042 g, 0.15 mmol). The yield of the colorless block crystals is ca. 59 % based on L. Elemental Anal. Found: C, 43.55; N, 9.19; H, 3.44 %. Calcd. for C₄₄H₄₂N₈O₁₅S₂Cd₂: C, 43.59; N, 9.25; H, 3.47 %. IR (cm⁻¹): 3385(s), 2226(m), 1609(s), 1559(m), 1540(m), 1506(w), 1484(m), 1442(w), 1399(m), 1322(w), 1279(w), 1222(w), 1111(s), 1034(s), 955(w), 833(m), 805(w), 683(w), 626(m), 502(w).

Synthesis of graphene/complex 1 composite: The synthesis of complex **1**/graphene composite was carried out as described above for complex **1** except that 0.5 mg graphene was extra added. The resulting black powder was filtered and characterized by powder XRD and SEM.

X-ray crystallography Single-crystal X-ray data for complexes **1-3** were collected on an Oxford XCalibur Eos diffractometer using graphite monochromated Mo K α (λ = 0.71073 Å) radiation at room temperature. Empirical absorption correction was applied. The structures were solved by direct methods and refined by the full-matrix least-squares methods on

F^2 using the SHELXTL-97 software.⁵ All non-hydrogen atoms were refined anisotropically. All of the hydrogen atoms were placed in the calculated positions. The crystal data and structure refinements for complexes **1-3** are summarized in **Table 1**. Selected bond lengths and angles for complexes **1-3** are listed in **Table S1** in the supporting information. Further details are provided in the supporting information. The CCDC reference numbers are the following: 1009274 for complex **1**, 1009275 for complex **2** and 1009276 for complex **3**.

Results and discussion

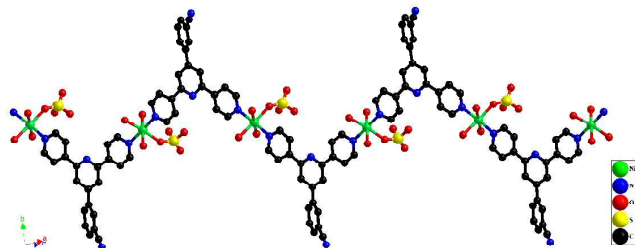
Synthesis Complexes **1-3** were prepared by solvothermal technique. The species of solvents were of crucial important for the crystallization of the aimed products. In the presence of individual water or individual ethanol, the crystals of complexes **1-3** can't be obtained. When the mixture of 1:1 water/ethanol was utilized, the crystals of complexes **1-3** are in good quality. However, the ratio of metal ion/ligand is not very important for the crystallization, it can be adjusted from 1:1 to 1:3.

Crystal Structure of M₂L₂(SO₄)₂(H₂O)₆·H₂O (M= Ni (1**), Co (**2**), Cd (**3**))** Complexes **1-3** are isostructural except for different metal(II) ions in the structures (**Table S1**). Therefore, we will describe the structure of the Ni complex **1** in comparison with those of Co complex **2** and Cd complex **3**. Complex **1** crystallizes in the *monoclinic* space group $P2_1/n$, its asymmetric unit contains one crystallographically unique Ni(II), one L, one SO₄²⁻, three coordinated water molecules and 0.5 uncoordinated water molecule. Due to the disorder, the phenyl ring and the -CN group from the L ligand are disordered over two locations, and their occupancy factors are 0.575 and 0.425, respectively. The SO₄²⁻ is disordered over two locations and each of them is half-occupied. One coordinated water molecule is disordered over two locations with 0.485 and 0.515 of occupancy factors, respectively. In complex **1**, the crystallographically independent Ni(II) exhibits a slightly distorted octahedral geometry, being defined by three O atoms from three aqua ligands and one O atom from SO₄²⁻ in the equatorial position and two pyridine atoms from two L ligands in the apical position [Ni-O 1.983(8) - 2.191(12) Å, Ni-N 2.123(3) - 2.124(3) Å] (**Fig.1a** and **Table S1**). In complexes **2** and **3**, the asymmetric unit contains two crystallographically unique metal (II), two L, two SO₄²⁻, six coordinated water molecules and one uncoordinated water molecule. In complex **2**, the Co-O and Co-N bond lengths are in the range of 2.073(4)-2.143(4) and 2.169(4) - 2.179(4) Å, respectively (**Table S1**). In complex **3**, the Cd-O and Cd-N bond lengths are in the range of 2.287(6)- 2.360(7) and 2.330(6) -2.343(7) Å, respectively (**Table S1**).

In the three complexes, L acts as a μ_2 -bridge connecting two metal (II) centers via its two terminal pyridine N atoms into a one-dimensional (1D) chain (**Fig. 1a**). In complex **1**, L is almost a planar molecule. The dihedral angles between the two neighboring pyridine rings of L are 7.5 and 2.4 °, respectively. And the dihedral angle between its neighboring phenyl ring and pyridine ring is 36.7 °. In complex **2**, the dihedral angles between the two neighboring aromatic rings of one crystallographically unique L ligand are 8.8, 8.1 and 37.8 °, respectively. As for another crystallographically unique L ligand, the dihedral angles

are 6.3, 2.3 and 36.4 °, respectively. In complex **3**, the dihedral angles for the two crystallographically unique **L** ligand are 8.8, 8.1, 37.8 and 8.5, 7.3, 38.0 °, respectively. Strong H bonds (Table 2) and π - π stacking interactions (Table 3) are observed in the three complexes, and the three complexes show a three-dimensional (3D) supramolecular architecture (Fig.1b).

(a)



(b)

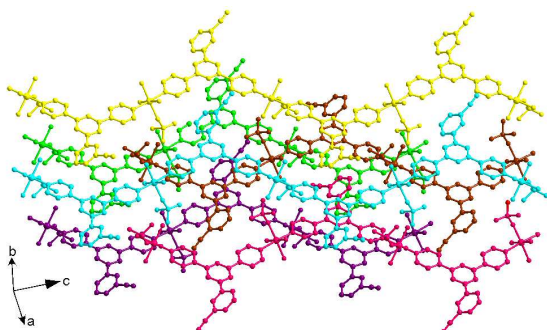
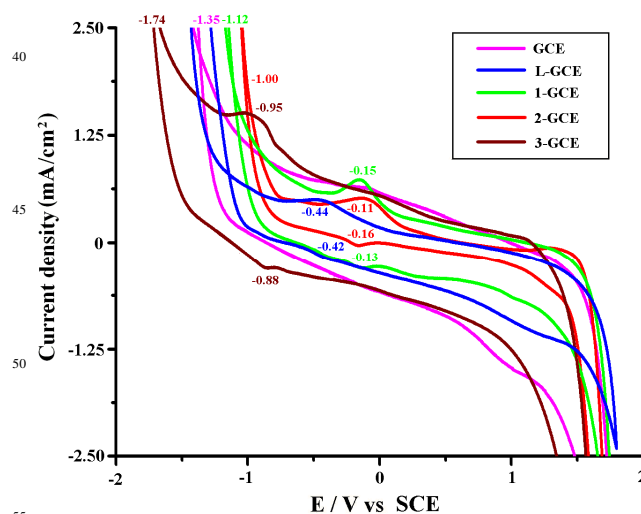


Fig.1. 1D chain constructed by Ni(II) and **L** in complex **1** (a); 1D chains are linked by strong π - π stacking interactions into 3D architecture (Different chains denoted in different colors) (b) (H atoms, disordered atoms and uncoordinated water molecules omitted for clarity).

The electrocatalytic Properties of Complexes 1 and 2 The powder XRD patterns of complexes **1-3** are shown in Fig. S1 in the supporting information. All the peaks of the three compounds can be indexed to their respective simulated XRD powder patterns, indicating each of the three compounds is pure phase.

CVs for the **1**-modified electrode (**1-GCE**), **2**-modified electrode (**2-GCE**), **3**-modified electrode (**3-GCE**), **L**-modified glassy carbon electrode (**L-GCE**) and the bare **GCE** were measured in a 0.5 M Na₂SO₄ (50 mL) solution at a scan rate of 10 mV·s⁻¹. As shown in Figs.2 and S2, the bare **GCE** exhibits electrochemical responses with proton reduction at an onset potential of approximately -1.35 V vs SCE. As we know, the theoretical potential for the H₂ evolution reaction (HER) in a neutral aqueous solution (pH=7) on a clean Pt electrode is -0.66 V vs SCE,⁶ indicating the overpotential for the HER in the blank system is -0.69 V vs SCE. The CV of the **L-GCE** at 10 mV·s⁻¹ showed similar electrochemical response with respect to the bare **GCE**, indicating the free ligand **L** almost can't catalyze the HER (Figs.2 and S3). The quasi-reversible waves at -0.44 and -0.42 V vs SCE are probably ascribed to the redox of the π electrons of **L** (Figs.2 and S3).

(a)



(b)

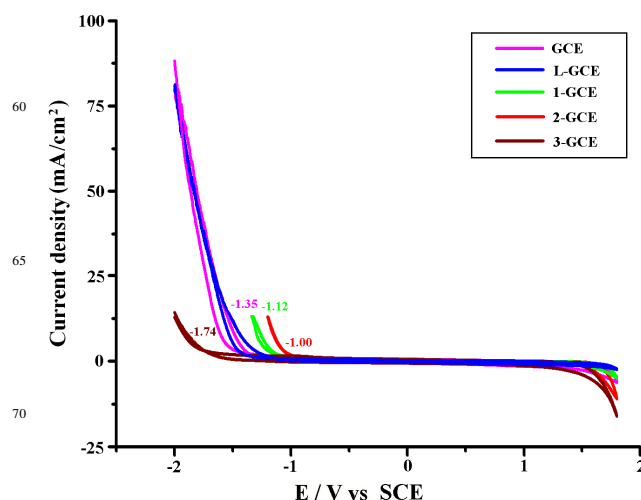


Fig.2 Cyclic voltammograms (CVs) of the bare **GCE**, **L-GCE**, **1-GCE**, **2-GCE** and **3-GCE** in 0.5 M Na₂SO₄ solution (50mL) at a sweep rate of 10 m V·s⁻¹ with the vertical axis denoted in different scales (a) (b).

The CV reveals the onset H⁺ reduction potential at the **1-GCE** is positively shifted to -1.12 V vs SCE ($\eta = -0.46$ V) accompanying with the enhanced HER current in respect to the bare **GCE** at a scan rate of 10 mV·s⁻¹ (Figs.2 and S4), inferring that complex **1** can act as an electrocatalyst for the generation of H₂.⁷ The quasi-reversible peaks at -0.15 and -0.13 V vs SCE may be related with the redox of the Ni(II) in complex **1** (Figs.2 and S4).

In order to investigate the effect of metal(II) ion on the electrocatalytic property for the HER, the electrochemical property of the Co complex **2** was also evaluated under similar condition. The CV reveals the onset of the proton reduction is positively shifted to -1.00 V vs SCE (overpotential $\eta = -0.34$ V) at the **2-GCE** accompanying with the enhanced HER current with respect to the bare **GCE** (Figs.2 and S5), indicating complex **2** can also electrocatalyze the HER from water. The quasi-reversible peaks at -0.11 and -0.16 V vs SCE may be due to the redox of the Co(II) in complex **2** (Figs.2 and S5).

As described above, the overpotential of H⁺ reduction at **2-GCE** (-0.34 V) is more positive than that at **1-GCE** (-0.46 V),

(Figs.2, S4 and S5), indicating the Co complex **2** possesses better catalytic activity for the HER than the Ni complex **1**. The result is also proved by the Tafel plots of the two electrodes. As shown in Fig.S6a, **2-GCE** shows lower overpotential and enhanced current for the HER than **1-GCE**. And much lowered HER overpotentials and much enhanced HER currents are observed at the two modified GCE than those at the bare GCE. As we know, $\eta = a + b \lg i$, $a = \lg i_0$, $b = -RT/(nF)$.⁸ As shown in Fig S6b, in the presence of complex **1**, it can be calculated the slope $b = -1.438$ and the intercept $a = -4.10$, then the charge-transfer efficiency $\alpha = 8.93 \times 10^{-3}$ and the exchanging current $i_0 = 7.94 \times 10^{-5}$ A. Whereas in the presence of complex **2**, $a = -5.0$, $b = -4.292$, $\alpha = 2.99 \times 10^{-3}$ and $i_0 = 1.0 \times 10^{-5}$ A.

In the presence of complexes **1** and **2**, at the onset potentials of -1.12 V and -1.00 V vs SCE, respectively, with the increase of scan rates, the ratio of the HER peak current i_p / square root of the scan rate $v^{1/2}$ is decreased (Figs.S4, S5 and S7), indicating the rate determining step of the hydrogen evolution is electrochemical reaction.^{8a}

The electrochemical impedance spectroscopy (EIS) allows us to explore the electrocatalytic mechanism of the two complexes.⁹ Fig.3 shows the Bode plots of **1-GCE**, **2-GCE** and the bare GCE at -1.1 V vs SCE. As shown in Fig.3, the R_s (electrolyte resistance) and R_{ct} (charge-transfer resistance) can be observed from the magnitude plot in the high and low frequency regions, respectively.⁹ According to the Bode plots, the R_{ct} values for the HER in the presence of complexes **1** and **2** are lower than that in the blank system, indicating the charge transfer is promoted in the presence of the two complexes, thus the current is enhanced in the presence of the complexes.⁹ Moreover, it is found that the R_{ct} value at **2-GCE** is lower than that at **1-GCE**, which can account for the better electrocatalytic property of complex **2** than complex **1**.

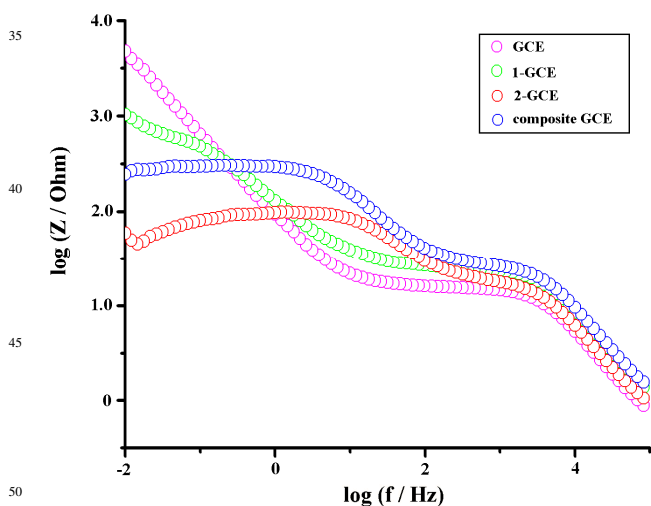


Fig. 3 Bode plots (log of impedance magnitude vs. log f) of the three-electrode systems in 0.5 M Na_2SO_4 solution (50mL) at the initial potential of -1.1 V with the bare GCE, **1-GCE**, **2-GCE** and composite-GCE as working electrodes, respectively.

Controlled potential electrolysis (CPE) experiments over 0.5 h at -1.1 V vs SCE ($\eta = -0.44$ V) also allow us to explore the catalytic activities of complexes **1** and **2** for the HER. As depicted in Fig.S8, **1-GCE** (current density = 1.74 mA/cm^2) and **2-GCE** (current density = 4.33 mA/cm^2) and show more favorable

electrochemical responses than the bare GCE under similar condition (current density = 1.34 mA/cm^2). And CPE experiments show the two catalysts for the HER both operate at 99 % Faradaic efficiencies (see ESI). The turnover numbers (TON) of 0.9 and 2.2 mol of H_2 per mole of complex **1** and **2** are calculated, respectively.

After CPE, the solid samples left on the electrodes (Fig.S9) are characterized by the powder X-ray diffractions (PXRD) (Fig.S1a-b), which are in agreement with their respective simulated PXRD patterns, indicating complexes **1** and **2** are stable under the HER condition.

The solution after CPE was characterized by UV-visible spectroscopy. It is found that the absorption spectra of the solution in the presence of **1-GCE** (Fig.S10a) or **2-GCE** (Fig.S10b) didn't change after electrolysis at -1.1 V vs for 2 h. And the blank Na_2SO_4 solution shows different UV-visible absorption from the Na_2SO_4 solution of **L** ligand, which exhibits an absorption peak at 225 nm (Fig. S10a), indicating complexes **1** and **2** weren't decomposed into metal(II) ions and **L** ligand during the electrocatalytic process for the HER.

Complexes **1** and **2** are stable electrocatalysts for the HER, which can be explained by the Nernst equation. As described above, the two complexes show 3D supramolecular architecture, in which 1D chains are linked by strong H bonds and π - π stacking interactions, the two complexes are almost insoluble in neutral aqueous solution. With the decrease of the concentration of metal(II) ions in the solution, $E(\text{M}^{2+}/\text{M})$ ($\text{M} = \text{Ni}$ or Co) is decreased. Then $E(\text{Co}^{2+}/\text{Co})$ can be less than $E(\text{H}^+/\text{H}_2)$, and metal(II) in complexes **1** and **2** can't be reduced into metal during the HER process. Thus the electrocatalyst is stable for the HER.^{3b}

The electrochemical Property of Complex 3 As described above, complexes **1** and **2** are isostructural except for different metal(II) ions in the frameworks. However, the two complexes possess different overpotentials for the HER from water, indicating the lowered HER overpotential is probably related with the metal center of electrocatalyst.¹⁰ In an attempt to further investigate the relationship between the metal(II) active center and the electrocatalytic activity for the HER, the electrochemical behavior of the Cd complex **3** was investigated under similar condition.

As shown in Fig.2, CV reveals a couple of quasi-reversible peaks at -0.95 and -0.88 V vs SCE at 10 $\text{mV}\cdot\text{s}^{-1}$, which may be related with the redox of the Cd(II) in complex **3** (Figs.2 and S11). The irreversible peak for the HER at the **3-GCE** is negatively shifted to -1.74 V vs SCE ($\eta = -1.08$ V) with lowered HER current in respect to the bare GCE (-1.35 V vs SCE, $\eta = -0.69$ V) (Figs.2 and S11), indicating complex **3** can't catalyze the production of H_2 . The present work further shows the species of metal(II) ions plays an important role in the electrocatalytic activity for the HER. And the sequence for the electrocatalytic activity is: Co complex > Ni complex > Cd complex. The detailed mechanism is under investigation.

The electrocatalytic Property of Complex 1/Graphene Composite Graphene, possesses extraordinary electron conductivity, thermal and mechanical properties, attracts people's extensive attention. In the present work, we synthesize complex

1/graphene composite to investigate its electrochemical property. Herein, graphene was commercially purchased from Nanjing XFNANO Materials Tech Co., Ltd, which exhibits graphene's characteristic Raman signals at approximately 1342 cm^{-1} (D peak), 1571 cm^{-1} (Q peak) and an overtone peak near 2682 cm^{-1} (2D peak) (Fig.S12).¹¹ The synthesis of complex 1/graphene composite was carried out as described above for complex 1 except that 0.5 mg graphene was extra added. The resulting black powder was filtered and characterized by powder XRD. It displays a PXRD pattern similar to that of complex 1 (Fig.S1a), indicating the black sample is the complex 1/graphene composite, which is also proved by the SEM images of the composite, as shown in Fig. S13.

Due to the light weight of graphene, only 0.3 mg graphene or 0.3 mg complex 1/graphene composite were used to cover the 0.2 cm^2 geometric area of the GCE to obtain the graphene-modified electrode (graphene-GCE) and complex 1/graphene composite-modified electrode (composite-GCE), respectively. Their CVs were measured in a 0.5 M Na_2SO_4 (50 mL) solution at different scan rates. As shown in Fig.4 and Fig. S14, no obvious HER wave is found in the range of -1.4-1.8 V vs SCE in the CV of the graphene-GCE at scan rates of 10, 20 or 50 $\text{mV}\cdot\text{s}^{-1}$, indicating the graphene can't catalyze the production of H_2 from water. However, when the composite-GCE is used as the working electrode instead, similar HER overpotential and current are observed with respect to the individual complex 1-modified GCE at scan rates of 10, 20 or 50 $\text{mV}\cdot\text{s}^{-1}$ (Figs.4 and S14), indicating the complex 1/graphene composite and the individual complex 1 possess similar electrocatalytic activity for the HER though the graphene can't catalyze the electrolysis of water, which is also evidenced by their Tafel plots (Fig.S6).

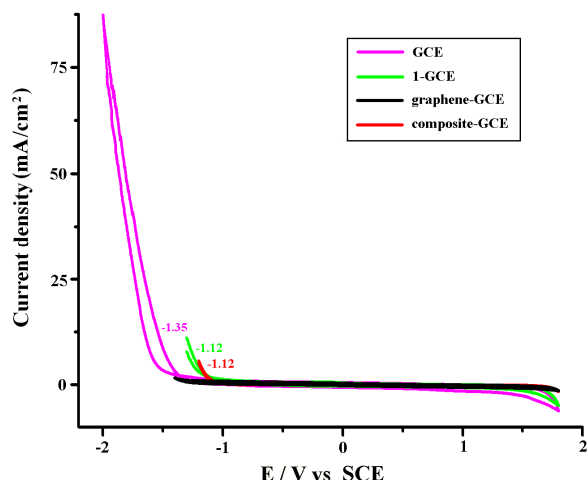


Fig.4 CVs of the bare GCE, 1-GCE, graphene-GCE and composite-GCE in 0.5 M Na_2SO_4 solution (50mL) at a sweep rate of 10 $\text{mV}\cdot\text{s}^{-1}$.

Usually, MOFs are not electroconductive, which limits their uses in electrochemical fields. Herein, though the graphene can't catalyze the HER from water, the complex 1/graphene composite shows good electrocatalytic activity, which may be ascribed to the synergistic effect of graphene and complex 1. Graphene possesses good electrical conductivity, which can make up for the insulating complex. As the Bode plots shown in Fig.3, the R_{ct} value for the HER in the presence of the graphene/complex 1 composite is lower than those in the blank system and in the presence of the individual complex 1, indicating the charge transfer is more promoted in the presence of the composite.⁹

As described above, due to the light weight of graphene, the usage of graphene can reduce the amount of the electrocatalyst of

complex 1 in the composite greatly, but doesn't lower the electrocatalytic activity of complex 1.

UV-vis Absorption Spectra The UV-vis absorption spectra of the free organic ligand L and complexes 1-3 at room temperature are shown in Fig. S15. As shown in Fig.S15, the free ligand L exhibits strong absorption peak at ca. 286 nm and a shoulder peak at 334 nm in the range of 230-800 nm, which may be ascribed to the $n\text{-}\pi^*$ or $\pi\text{-}\pi^*$ transition.¹² Complex 1 displays two absorption peaks at ca. 270 and 328 nm in the range of 230-500 nm. In the similar range, complex 2 exhibits absorption peaks at ca. 260 and 323 nm. As for complex 3, its absorption peaks are observed at ca. 272 and 325 nm. The absorption peaks for complexes 1-3 are different from those of L, indicating they may be ascribed to the intraligand transition (ILCT) or metal-to-ligand charge-transfer transition (MLCT).¹² In the range of 450-800 nm, complexes 1 and 2 show absorption peaks at ca. 622 and 504 nm, respectively, they may be ascribed to the visible $d-d$ transition (Fig. S15).

Photoluminescence Property The photoluminescence properties of the Cd(II) complex 3 together with the free ligand L were studied in the solid state at room temperature. The emission spectra of the complex and the free organic ligand (slit width = 5nm) are depicted in Fig. S16. L displays an intense emission peak at 410 nm ($\lambda_{\text{ex}} = 340$ nm), which may be ascribed to the $\pi^*\text{-}n$ or $\pi\text{-}\pi^*$ transitions.¹³ Complex 3 displays emission band at 400 nm with an excitation band at 320 nm (Fig. S16), which is different from that of the free ligand L, which may be assigned to the LLCT, admixing with the LMCT as previously reported.¹⁴ The reduction of emission intensity in the complex may be attributed to the coordination of ligand to Cd(II) center, which enhances the loss of energy through a radiationless pathway.¹⁵

Thermal stability In order to examine the thermal stabilities of the three complexes, thermogravimetric analyses (TGA) were carried out. The samples were heated up to 750 $^{\circ}\text{C}$ in N_2 .

The TGA curve of complex 1 shows weight loss of 1.8 % in the range of 25-100 $^{\circ}\text{C}$, corresponding to the loss of the uncoordinated water molecules (calc. 1.6 wt%), and complex 1 loses its coordinated water molecules in the range of 110-210 $^{\circ}\text{C}$ (obsd. 9.8 %; calc. 9.6 wt %) (Fig. S17). Complex 2 shows one step of total weight loss of 11.6 % in the range of 25-160 $^{\circ}\text{C}$, corresponding to the loss of the uncoordinated and coordinated water molecules (calc. 11.4 wt %). The dehydrated sample remained stable up to ~310 $^{\circ}\text{C}$ without any weight loss (Fig.S17). As for complex 3, the loss of uncoordinated and coordinated water molecules (obsd, 10.4 %; calcd, 10.4%) happens in the range of 25-220 $^{\circ}\text{C}$. Decomposition of the dehydrated sample began at 220 $^{\circ}\text{C}$, in the temperature range 220–600 $^{\circ}\text{C}$ with a loss of 77.8 wt% (calc. 78.0 wt%). The decomposition process ended at about 600 $^{\circ}\text{C}$ (Fig.S17).

Conclusion

Based on L, three isostructural metal(II) complexes have been synthesized and structurally characterized by single-crystal X-ray diffraction. The three complexes all exhibit 3D supramolecular architecture, in which the L ligand acts as a μ_2 -bridge linking two

metal(II) centers into 1D chain, and different chains are connected by strong H bonds and π - π stacking interactions. Among the three complexes, the Ni complex **1** and Co complex **2** can act as the electrocatalysts for the HER from water, whereas the Cd(II) complex **3** can't. The Co complex **2** shows better electrocatalytic activity than the Ni complex **1**. The present work shows the species of metal(II) ions plays an important role in the electrocatalytic activity for the HER, which probably function as the active centers for the binding of intermediate species.¹⁰ In our work, the graphene can't catalyze the HER, however, the complex **1**/graphene composite shows similar electrocatalytic activity to complex **1**, it is probably due to the synergistic effect of graphene and complex **1**. Graphene has good electrical conductivity, which can make up for the insulating complex. The usage of graphene can reduce the amount of complex **1** in the composite greatly, but doesn't lower the electrocatalytic activity of the electrocatalyst.

Financial supports from the National Natural Science Foundation of China (No. 21371184), the Fundamental Research Funds for the Central Universities (No. CQDXWL-2012-024) and Chongqing Key Laboratory of Chemical Process for Clean Energy and Resource Utilization are gratefully acknowledged.

Notes and references

^aDepartment of Applied Chemistry, College of Chemistry and Chemical Engineering, Chongqing University, Chongqing 400030, P. R. China Tel: +86-023-65106150 E-mail: gongyun7211@cqu.edu.cn

^bZhejiang University, Hangzhou 310058, P. R. China Tel: +86-0571-88981583 E-mail: jhlin@zju.edu.cn; jhlin@cqu.edu.cn; jhlin@pku.edu.cn

† Electronic Supplementary Information (ESI) available: [Crystallographic data; PXRD patterns; CVs; Tafel plots; UV-vis absorption spectra; Raman spectrum; SEM images; TG curves; solid-state emission spectra and other supplementary material]. See DOI: 10.1039/b000000x/

References

- (a) M. W. Hosseini, *Acc. Chem. Res.*, 2005, **38**, 313; (b) P. J. Steel, *Acc. Chem. Res.*, 2005, **38**, 243; (c) C. Janiak, *Coord. Chem. Rev.*, 2006, **250**, 66; (d) F. Blank and C. Janiak, *Coord. Chem. Rev.*, 2009, **253**, 827; (e) X. C. Huang, Y. Y. Lin, J. P. Zhang and X. M. Chen, *Angew. Chem. Int. Ed.*, 2006, **45**, 1557; (f) Q. R. Fang, G. S. Zhu, Z. Jin, M. Xue, X. Wei, D. J. Wang and S. L. Qiu, *Angew. Chem. Int. Ed.*, 2006, **45**, 6126; (g) S. T. Zheng, J. Zhang, X. X. Li, W. H. Fang and G. Y. Yang, *J. Am. Chem. Soc.*, 2010, **132**, 15102.
- (a) A. Walcarius, *Chem. Soc. Rev.*, 2013, **42**, 4098; (b) R. W. Murray, *Molecular Design of Electrodes Surfaces*, Techniques of Chemistry, Wiley, New York, 1992, **22**, 1; (c) J. Wang, *Electroanalysis*, 1991, **3**, 255; (d) J. A. Cox, M. E. Tess and T. E. Cummings, *Rev. Anal. Chem.*, 1996, **15**, 173; (e) J. Labuda, M. Vanickova, M. Buckova and E. Korgova, *Chem. Pap.*, 2000, **54**, 95; (f) I. Svančara, K. Kalcher, A. Walcarius and K. Vytras, *Electroanalysis with Carbon Paste Electrodes*, CRC Press, Taylor & Francis Group, Boca Raton, FL, 2012, 1.
- (a) Y. Gong, H. F. Shi, Z. Hao, W. Hua and J. H. Lin, *Cryst. Growth Des.*, 2014, **14**, 649; (b) Y. Gong, Z. Hao, H. F. Shi, P. G. Jiang, M. M. Zhang and J. H. Lin, *ChemPlusChem*, 2014, **79**, 266; (c); Y. Gong, H. F. Shi, Z. Hao, J. L. Sun and J. H. Lin, *Dalton Trans.* 2013, **42**, 12252; (d) Y. Gong, T. Wu, P. G. Jiang, J. H. Lin and Y. X. Yang, *Inorg. Chem.*, 2013, **52**, 777.
- K. Hiroki and N. Toshi, *Chem. Eur. J.*, 2012, **18**, 1781.
- (a) G. M. Sheldrick, *SHELXS 97, Program for Crystal Structure Solution*, University of Göttingen, Göttingen, Germany, 1997. (b) G. M. Sheldrick, *SHELXL 97, Program for Crystal Structure Refinement*, University of Göttingen, Göttingen, Germany, 1997.
- B. Nohra, H. E. Moll, L. M. R. Albelo, P. Mialane, J. Marrot, C. M. Draznieks, M. O'Keeffe, R. N. Biboum, J. Lemaire, B. Keita, L. Nadjo and A. Dolbecq, *J. Am. Chem. Soc.*, 2011, **133**, 13363.
- (a) L. Cheng, X. M. Zhang, X. D. Xi and S. J. Dong, *J. Electroanal. Chem.* 1996, **407**, 97; (b) X. L. Wang, C. Qin, E. B. Wang, Z. M. Su, Y. G. Li and L. Xu, *Angew. Chem. Int. Ed.*, 2006, **45**, 7411; (c) P. P. Zhang, J. Peng, H. J. Pang, J. Q. Sha, M. Zhu, D. D. Wang and M. G. Liu, *CrystEngComm*, 2011, **13**, 3832; (d) L. F. Yang, S. Kinoshita, T. Yamada, S. Kanda, H. Kitagawa, M. Tokunaga, T. Ishimoto, T. Ogura, R. Nagumo, A. Miyamoto and M. Koyama, *Angew. Chem. Int. Ed.*, 2010, **49**, 5348; (e) X. L. Wang, H. L. Hu, G. C. Liu, H. Y. Lin and A. X. Tian, *Chem. Commun.*, 2010, **46**, 6485.
- (a) H. Yang and W. Q. Lu, *Applied electrochemistry*, Science press, Beijing, 2001, 46; (b) Y. Gao and B. Wu, *Electrochemical Basis*, Chemical industry press, Beijing, 2003, 53.
- (a) M. Hunsom, *Spectrosc. Prop. Inorg. Organomet. Compd.*, 2012, **42**, 196; (b) S. A. Mamuru, K. I. Ozoemena, T. Fukuda and N. Kobayashi, *J. Mater. Chem.*, 2010, **20**, 10705; (c) S. Ghosh, R. K. Sahu and C. R. Raj, *J. Mater. Chem.*, 2011, **21**, 11973; (d) M. K. Datta, K. Kadakia, O. I. Velikokhatnyi, P. H. Jampani, S. J. Chung, J. A. Poston, A. Manivannan and P. N. Kumta, *J. Mater. Chem. A*, 2013, **1**, 4026; (e) R. N. Reddy and R. G. Reddy, *J. Power Sources*, 2004, **132**, 315.
- Koper, M. T. M.; Bouwman, E. *Angew. Chem. Int. Ed.*, 2010, **49**, 3723.
- (a) H. Liu, S. Ryu, Z. Y. Chen, M. L. Steigerwald, C. Nuckolls and L. E. Brus, *J. Am. Chem. Soc.*, 2009, **131**, 17099; (b) E. Pollak, B. S. Geng, K. J. Jeon, I. T. Lucas, T. J. Richardson, F. Wang and R. Kostecki, *Nano Lett.*, 2010, **10**, 3386.
- (a) S. Ohkoshi, H. Tokoro, T. Hozumi, Y. Zhang, K. Hashimoto, C. Mathonière, I. Bord, G. Rombaut, M. Verelst, C. C. Moulin and F. Villain, *J. Am. Chem. Soc.*, 2006, **128**, 270; (b) M. Stadler, F. Puntoriero, S. Campagna, N. Kyritsakas, R. Welter and J. M. Lehn, *Chem. Eur. J.*, 2005, **11**, 3997; (c) J. H. Wang, Y. Q. Fang, L. Bourget-Merle, M. I. J. Polson, G. S. Hanan, A. Juris, F. Loiseau and S. Campagna, *Chem. Eur. J.*, 2006, **12**, 8539.
- (a) L. Y. Zhang, J. P. Zhang, Y. Y. Lin and X. M. Chen, *Cryst. Growth Des.*, 2006, **6**, 1684; (b) Q. Shi, Y. T. Sun, L. Z. Sheng, K. F. Ma, M. L. Hu, X. G. Hu and S. M. Huang, *Cryst. Growth Des.*, 2008, **8**, 3401; (c) R. B. Zhang, Z. J. Li, Y. Y. Qin, J. K. Cheng, J. Zhang and Y. G. Yao, *Inorg. Chem.*, 2008, **47**, 4861; (d) Y. H. He, Y. L. Feng, Y. Z. Lan and Y. H. Wen, *Cryst. Growth Des.*, 2008, **8**, 3586.
- (a) S. L. Zheng, M. L. Tong, S. D. Tan, Y. Wang, J. X. Shi, Y. X. Tong, H. K. Lee and X. M. Chen, *Organometallics*, 2001, **20**, 531; (b) B. Valeur, *Molecular Fluorescence: Principles and Applications*; Wiley-VCH: Weinheim, Germany, 2002; (c) H. Y. He, D. Collins, F. N. Dai, X. L. Zhao, G. Q. Zhang, H. Q. Ma and D. F. Sun, *Cryst. Growth Des.*, 2010, **10**, 895; (d) Y. Liu, P. F. Yan, Y. H. Yu, G. F. Hou, J. S. Gao and J. Y. Lu, *Cryst. Growth Des.*, 2010, **10**, 1559.
- (a) S. R. Fan and L. G. Zhu, *Inorg. Chem.*, 2007, **46**, 6785; (b) J. R. Berenguer, A. Díez, J. Fernández, J. Forníés, A. García, B. Gil, E. Lalinde and M. T. Moreno, *Inorg. Chem.*, 2008, **47**, 7703; (c) S. H. Li, S. K. Gao, S. X. Liu and Y. N. Guo, *Cryst. Growth Des.*, 2010, **10**, 495; (d) H. Yin and S. X. Liu, *Inorg. Chem. Commun.*, 2009, **12**, 187; (e) K. Lyczko, W. Starosta and I. Persson, *Inorg. Chem.*, 2007, **46**, 4402; (f) R. Ferreira-Martínez, D. Esteban-Gómez, C. Platas-Iglesias, A. Blas and T. Rodríguez-Blas, *Dalton Trans.*, 2008, 5754.

Table 1 Crystal data and structure refinements for complexes **1-3**

| Complex | 1 | 2 | 3 |
|---|--|---|---|
| Empirical formula | C ₄₄ H ₄₂ Ni ₂ N ₈ O ₁₅ S ₂ | C ₄₄ H ₄₂ Co ₂ N ₈ O ₁₅ S ₂ | C ₄₄ H ₄₂ Cd ₂ N ₈ O ₁₅ S ₂ |
| <i>M</i> | 1104.38 | 1104.84 | 1211.82 |
| Crystal system | Monoclinic | Monoclinic | Monoclinic |
| Space group | <i>P</i> 2 ₁ / <i>n</i> | <i>P</i> 2 ₁ / <i>c</i> | <i>P</i> 2 ₁ / <i>n</i> |
| <i>a</i> /Å | 7.286(8) | 14.6160(14) | 14.8543(14) |
| <i>b</i> /Å | 12.218(14) | 12.1893(11) | 12.3149(11) |
| <i>c</i> /Å | 24.76(3) | 25.892(3) | 26.163(3) |
| α /° | 90 | 90 | 90 |
| β /° | 90.484(14) | 106.274(2) | 106.126(2) |
| γ /° | 90 | 90 | 90 |
| <i>V</i> /Å ³ | 2204(4) | 4428.1(7) | 4597.7(8) |
| <i>Z</i> | 2 | 4 | 4 |
| <i>D</i> _{calc} /g cm ⁻³ | 1.664 | 1.657 | 1.751 |
| μ /mm ⁻¹ | 1.033 | 0.927 | 1.096 |
| No. of unique reflns | 3630 | 3585 | 3521 |
| reflns used [<i>I</i> > 2 σ (<i>I</i>)] | 3630 | 3585 | 3521 |
| F(0 0 0) | 1140 | 2272 | 2440 |
| Goodness-of-fit on <i>F</i> ² | 1.035 | 1.054 | 1.098 |
| Final <i>R</i> indices | <i>R</i> ₁ = 0.0468 [<i>I</i> > 2 σ (<i>I</i>)] <i>wR</i> ₂ = 0.1052 | <i>R</i> ₁ = 0.0553, <i>wR</i> ₂ = 0.1146 | <i>R</i> ₁ = 0.0595, <i>wR</i> ₂ = 0.1384 |

$$R_1 = \sum ||F_o| - |F_c|| / \sum |F_o|; wR_2 = \sum [w(F_o^2 - F_c^2)^2] / \sum [w(F_o^2)]^{1/2}$$

Table 2 Distances (Å) and angles (°) of the selected hydrogen bonds in complexes **1-3**

| D | H | A | D...A distance | H...A distance | \angle D-H...A |
|------------------|------|-------|----------------|----------------|------------------|
| Complex 1 | | | | | |
| O6 | H6C | O3'#1 | 2.884 | 2.084 | 157 |
| O6 | H6C | O3#1 | 2.924 | 2.091 | 166 |
| O6 | H6D | O1 | 2.630 | 2.013 | 129 |
| O7 | H7C | O2#1 | 2.801 | 1.984 | 161 |
| O7 | H7D | O3#2 | 2.882 | 2.065 | 161 |
| O7 | H7D | O3'#2 | 2.855 | 2.081 | 151 |
| Complex 2 | | | | | |
| O9 | H9D | O8#3 | 2.814 | 2.122 | 138 |
| O10 | H10C | O3 | 2.663 | 1.838 | 163 |
| O10 | H10D | O7#4 | 2.722 | 1.897 | 163 |
| O11 | H11C | O8#4 | 2.725 | 1.876 | 177 |
| O12 | H12C | O4 | 2.987 | 2.157 | 165 |
| O12 | H12D | O7 | 2.821 | 1.993 | 165 |
| O13 | H13C | O3 | 2.653 | 1.839 | 160 |
| O13 | H13D | O4#4 | 2.906 | 2.091 | 161 |
| O14 | H14D | O4#4 | 2.781 | 1.997 | 153 |
| Complex 3 | | | | | |
| O9 | H9C | O2 | 2.797 | 1.976 | 162 |
| O9 | H9D | O7 | 2.748 | 1.927 | 162 |
| O10 | H10C | O6 | 2.662 | 1.847 | 160 |
| O10 | H10D | O7#2 | 2.772 | 1.957 | 160 |
| O11 | H11C | O5#2 | 2.828 | 1.979 | 177 |
| O12 | H12C | O3#1 | 2.796 | 2.107 | 138 |
| O13 | H13D | O3#2 | 2.731 | 1.882 | 177 |
| O14 | H14C | O6 | 2.734 | 1.916 | 161 |
| O14 | H14D | O2#2 | 2.689 | 1.870 | 161 |

^s Symmetry transformations used to generate the equivalent atoms:

#1: *x*+1, *y*, *z*; #2: -*x*+1/2, *y*+1/2, -*z*+1/2; #3: *x*-1, *y*, *z*; #4: -*x*+1, *y*-1/2, -*z*+1/2

Table 3 The centroid-centroid (CC) distance (Å) and perpendicular (P) distance (Å) involving $\pi \cdots \pi$ stacking interactions for complexes **1-3**

| Plane | Plane | CC distance | P distance |
|------------------|---------------|-------------|------------|
| Complex 1 | | | |
| N1/C1-C5 | N3A/C11A-C15A | 3.902(7) | 3.472(3) |

| | | | |
|------------------|----------------|----------|----------|
| N2/C6-C10 | N3B/C11B-C15B | 3.887(7) | 3.470(4) |
| C16-C21 | C16D-C21D | 3.702(8) | 3.419(5) |
| C16-C21 | C16E-C21E | 3.906(8) | 3.543(5) |
| <i>Complex 2</i> | | | |
| N5/C23-C27 | N6F/C28F- C32F | 3.931(3) | 3.484(2) |
| N6/C28- C32 | N2G/C6G-C10G | 3.724(4) | 3.392(3) |
| N7/C33- C37 | N3G/C11G-C15G | 3.993(4) | 3.484(3) |
| C38 -C43 | C38H -C43H | 3.690(4) | 3.460(3) |
| C38 -C43 | C16I-C21I | 3.667(4) | 3.398(3) |
| N1/C1- C5 | N3J/C11J-C15J | 3.876(4) | 3.461(3) |
| <i>Complex 3</i> | | | |
| N1/C1-C5 | N2K/C6K-C10K | 3.951(5) | 3.557(3) |
| N2/C6-C10 | N7K/C33K-C37K | 3.675(5) | 3.424(4) |
| N3/C11- C15 | N6K/C28K-C32K | 3.975(5) | 3.518(4) |
| C16 -C21 | C16L -C21L | 3.743(6) | 3.516(4) |
| C16 -C21 | C38L-C43L | 3.675(6) | 3.443(4) |
| N5/C23-C27 | N6M/C28M-C32M | 3.925(5) | 3.513(4) |

Symmetry transformations used to generate equivalent atoms:

A 2-x, 2-y, 1-z B 1-x, 2-y, 1-z D 1-x, 1-y, 1-z E 2-x, 1-y, 1-z F 1-x, -y, -z G 1-x, -1/2+y, 1/2-z H 1-x, -1-y, -z
I 1-x, -3/2+y, 1/2-z J -x, 1-y, 1-z K -x, 2-y, -z L -x, 3-y, -z M 1-x, 2-y, -z

Metal(II) complexes based on 4-(2,6-di(pyridin-4-yl)pyridin-4-yl)benzotrile: structures and electrocatalytic properties for hydrogen evolution reaction from water

Xiao Lin Gao, Yun Gong,* Pan Zhang, Yong Xi Yang, Jiang Ping Meng, Miao Miao Zhang, Jun Li Yin and Jian Hua Lin*

Using a novel rigid ditopic ligand, 4-(2,6-di(pyridin-4-yl)pyridin-4-yl)benzotrile (**L**), three metal(II)-complexes formulated as $M_2L_2(SO_4)_2(H_2O)_6 \cdot H_2O$ ($M=Ni$ (**1**), Co (**2**) and Cd (**3**)) have been solvothermally synthesized and structurally characterized by single-crystal X-ray diffraction. The three complexes are isostructural except for different metal(II) ions in the structures. They all show a one-dimensional (1D) chain, in which the **L** ligand acts a μ_2 -bridge linking two metal(II) centers. Different chains are connected by strong H bonds and π - π stacking interactions into three-dimensional (3D) supramolecular architecture. Among the three complexes, the Ni complex **1** and Co complex **2** can act as the electrocatalysts for hydrogen evolution reaction (HER) from water, and the Co complex **2** shows better electrocatalytic activity. In the present work, the graphene can't catalyze the HER, however, the complex **1**/graphene composite shows similar electrocatalytic activity to complex **1**. The three complexes show different UV-vis absorption, photoluminescence properties and thermal stabilities.

